Effects of discharge, wind, and tide on sedimentation in a recently restored tidal freshwater wetland

Verschelling, Eelco; van der Deijl, Eveline; van der Perk, Marcel; Sloff, Kees; Middelkoop, Hans

DOI
10.1002/hyp.11217

Publication date
2017

Document Version
Final published version

Published in
Hydrological Processes: an international journal

Received: 14 November 2016 | Accepted: 27 April 2017

DOI: 10.1002/hyp.11217

WILEY

RESEARCH ARTICLE

Effects of discharge, wind, and tide on sedimentation in a recently restored tidal freshwater wetland

Eelco Verschelling[1,2] | Eveline van der Deijl[1] | Marcel van der Perk[1] | Kees Sloff[2,3] | Hans Middelkoop[1]

[1] Department of Physical Geography, Utrecht University, Utrecht, The Netherlands

[2] Deltares, Delft, The Netherlands

[3] Department of Hydraulic Engineering, Delft University of Technology, Delft, The Netherlands

Correspondence
Eelco Verschelling, Department of Physical Geography, Utrecht University, Utrecht, The Netherlands.
Email: e.verschelling@uu.nl

Funding information
Dutch Technology Foundation STW, Grant/Award Number: 12431

Abstract

Sediment deposition is one of the key mechanisms to counteract the impact of sea level rise in tidal freshwater wetlands (TFWs). However, information about sediment deposition rates in TFWs is limited, especially for those located in the transition zone between the fluvially dominated and tidally dominated sections of a river delta where sedimentation rates are affected by the combined impact of river discharge, wind, and tides. Using a combined hydrodynamic–morphological model, we examined how hydrometeorological boundary conditions control sedimentation rates and patterns in a TFW located in the Rhine–Meuse estuary in the Netherlands. The modelling results show that net sedimentation rate increases with the magnitude of the river discharge, whereas stronger wind increasingly prevents sedimentation. Sediment trapping efficiency decreases for both increasing river discharge and wind magnitude. The impact of wind storms on the trapping efficiency becomes smaller for higher water discharge. The spatial sedimentation patterns are affected by all controls. Our study illustrates the importance of evaluating both the separate and the joint impact of discharge, wind, and tides when estimating sedimentation rates in a TFW affected by these controls. Such insights are relevant to design measures to reactivate the sedimentation process in these areas.

KEYWORDS

De Biesbosch National Park, morphodynamics, numerical modelling, sediment deposition, tidal freshwater wetlands

1 | INTRODUCTION

Tidal freshwater wetlands (TFWs) are home to characteristic and diverse vegetation communities and animal species, and their protection is thus important from a biodiversity conservation perspective. Wetlands also provide various ecosystem services to human well-being, for example, the provision of food (e.g., fish) and recreational opportunities, and regulating water quality (Millennium Ecosystem Assessment, 2005). TFWs are vulnerable to sea level rise (SLR) through both increased risk of inundation and possible salt water intrusion (e.g., Anderson & Lockaby, 2012; Burkett & Kusler, 2000).

Enhanced sedimentation is considered an effective strategy to prevent further wetland loss in case horizontal wetland migration to higher zones is not possible (Darke & Megonigal, 2003; Kirwan & Megonigal, 2013; Paola et al., 2011). Previous research has indicated that sedimentation rates of wetlands may in general be controlled by factors such as the supply of fluvial sediments (Neubauer, Anderson, Constantine, & Kuehl, 2002; Siobhan Fennessy, Brueske, & Mitsch, 1994), tide, wind (Delgado, Hensel, Swarth, Ceroni, & Boumans, 2013; Orson, Simpson, & Good, 1990), vegetation cover (Brueske & Barrett, 1994; Darke & Megonigal, 2003; Nardin & Edmonds, 2014; Nardin, Edmonds, & Fagherazzi, 2016; Pasternack & Brush, 2001), wetland shape properties such as average depth/wetland elevation, distance to tidal creeks, and wind fetch lengths (Hupp & Bazemore, 1993; Hupp, Demas, Kroes, Day, & Doyle, 2008; Mitsch et al., 2014; Temmerman, Govers, Wartel, & Meire, 2003b).

Yet little research has focused on TFWs located in the transition zone between the *fluvially dominated* and *tidally dominated* sections of a river delta (terms in italic as defined by Leonardi, Kolker, & Fagherazzi, 2015), where sedimentation rates are controlled by the combined impact of discharge, wind, and tide. The majority of previous studies has focused on cases where only one or two of these controls are relevant, for example, to study the relation between (1a) stationary water discharges and sediment deposition in a synthetic TFW (Nardin & Edmonds, 2014); (b) tidal ranges, sediment concentrations and bed-level changes in a TFW in the Scheldt estuary, Belgium/Netherlands (Temmerman, Govers, Meire, & Wartel, 2003a); and (c) wind waves and resuspension on a tidal mudflat in Willipa Bay, USA (Mariotti & Fagherazzi, 2013). However, a more thorough understanding of the combined impact of these hydrometeorological controls is essential to develop successful sedimentological restoration strategies in TFWs in the transition zone of a delta.

The objective of this study was to quantify and understand how sedimentation rates and patterns of mud and sand in TFW are affected by the interplay of river discharge, wind waves, and tide. To this end, we carried out numerical experiments using a hydrodynamic and sediment transport model of a recently restored, sparsely vegetated TFW in the south-western part of the Netherlands. We conducted 14 simulations with varying discharge, wind magnitude, and tidal conditions, and compared average surface accretion, trapping efficiency (defined as the proportion of the incoming sediment that is deposited or trapped in the area), and sedimentation patterns. This study concentrates on the first stage of renewed sedimentation of the TFW after the opening of the levees. Therefore, the effect of vegetation on the vertical mass balance (through increased sedimentation of suspended material and possible accretion due to production of organic material) is not considered.

This study took place within the framework of a larger project on the effects of restoring sedimentation in a former polder area, in which field measurements were carried out (water levels, flow velocities, turbidity, sediment concentrations, settling velocities, and sediment thickness). These measurements were used for the model set-up and calibration. The measurement programme and results will be described in a separate paper in preparation.

2 | STUDY AREA

The study area is located in the eastern section of *De Biesbosch* National Park, a 9,000 ha TWF in the lower part of the Rhine–Meuse delta in the Netherlands. The study area comprises three former polders (*Spiering*, *Kleine Noordwaard*, and *Maltha*) and has a surface area of around 700 ha. It was depoldered in 2008 by the park authority (State Forestry Service or *Staatsbosbeheer* in Dutch) as part of an ongoing programme to reduce flood water levels by enlarging inundation areas and to restore former wetland areas. Not only is this area itself potentially threatened by future SLR and, as such, a relevant case, the depoldering also created an excellent research environment to study sedimentation processes due to the size of the area and the limited number of in- and outlets, which facilitated the establishment of water and sediment balances.

The embankment around the polder was opened at two locations: on the northern side along the river *Nieuwe Merwede* (a major Rhine branch) close to location g1 in Figure 1, and on the southern side along the *Gat van de Noorderklip* (location g4), a smaller branch that connects with the *Hollands Diep* estuary. The dominant flow direction through the study area is from the North to the South. The area consists of inundated flats (former grassland and arable fields), a man-made channel system connecting the northern and southern in- and outlets, and a vegetated island in the centre of *Kleine Noordwaard*, which was constructed using the material dug from the channels. The substrate in the study area consists of a clay layer on top of a thick layer of fluvial-tidal splay sands (Kleinhans, Weerts, & Cohen, 2010). Artificial channels were dug through this clay layer into the sandy layer underneath.

The hydraulic regime in the study area is semidiurnal microtidal with an average tidal range of 0.2 to 0.4 m. Because the TFW is located in the backwater of the North Sea, water levels in the TFW are influenced by storm surges as a result of heavy westerly wind storms at sea and the operation settings of the Haringvliet barrier (between Hollands Diep and the North Sea). The water levels are also affected by the discharge of the Rivers Rhine and Meuse. Most of the time, the tidal flats are inundated with depths ranging from 0 to 50 cm. Complete exposure of the flats only occurs in summer (when river discharge is low) at low tide or during strong easterly winds. The wave climate within the area is characterized by local short waves generated by winds mainly coming from the west–south-west. The significant wave height during windstorm events was observed to grow up to 0.2 m, as a result of the relatively long fetch lengths across the inundated flats and the distinct lack of vegetation, especially in winter. However, the development of the waves is hampered by the low water depths that occur during low tides or low river discharge.

The suspended sediment concentration (SSC) in the Nieuwe Merwede typically varies from 10 to 40 mg/L during average flow conditions with estimated peak values of up to 140 mg/L during periods of high discharge in the River Rhine (Asselman, 2000; Asselman, Middelkoop, & van Dijk, 2003).

Bedload transport of coarser material dominates the changes in the channels' bed, especially close to the in- and outlets of the system where the flow velocities can reach values of up to 2 m/s. The flats have remained relatively unchanged due to the high erosion resistance of the thick clay layer of this former polder and the low flow velocities here (0 to 0.2 m/s). Since the opening of the area in 2008, the flats have become gradually covered by a layer of mud of around 2 to 5 cm thick.

Dominant vegetation types in the study area include bulrush vegetation with *Schoenoplectus triqueter* and *Bolboschoenus maritimus* on the shoreline, pioneer species such as *Limosella aquatica*, *Veronica anagallis-aquatica*, and *Pulicaria vulgaris* on the mud flats, and locally some *Myriophyllum spicatum* in open water. The vegetation on the flats is regularly cut in order to keep the hydraulic roughness low, thereby maintaining the flood-conveying capacity of the area. The area has become an important habitat for many bird species. Large flocks of geese frequently spend time in the Biesbosch area to feed on the vegetation, effectively removing most of it.

3 | METHODS

3.1 | Model set-up

We used Delft3D (Lesser, Roelvink, van Kester, & Stelling, 2004) to model hydrodynamics, sediment transport, and bed-level changes in the study

area. The following sections describe the set-up of the model domain and the modules for hydrodynamics, sediment transport, and morphology.

3.1.1 | Model domain and bathymetry

The computational grid covers the polders Spiering, Kleine Noordwaard, and Maltha (Figure 1). The land boundary largely follows the highest point of the original embankment around the polders. The upstream and downstream boundaries were chosen to coincide with the locations of fixed monitoring stations. The resolution and grid orientation were defined to account for dominant flow directions and important features in bathymetry (e.g., channels, island, in- and outlets). This resulted in a curvilinear grid of 144 × 145 cells, with cell sizes varying from 5 to 30 m (Figure 2).

The initial bathymetry of the model area was constructed using the 2003 version of the official Dutch DEM "AHN1" with a horizontal resolution of 5 × 5 m^2 (Van der Zon, 2013), supplemented by a local LIDAR DEM with a horizontal resolution of 1 × 1 m^2 from 2010 for the central island and other artificially elevated areas, and a 2011 multibeam echosounder dataset covering the channel system. All bathymetric data sets were provided by the National Water Authority (*Rijkswaterstaat*).

3.1.2 | Hydrodynamics

Delft3D-FLOW calculates water levels and water flow velocities for every computational time step on spherical or orthogonal curvilinear coordinates by solving the unsteady shallow water equations in two or three dimensions. For this study, we used a curvilinear grid and a computational time step of 30 s. Given the explorative character of this study, the small gradient over observed vertical sediment concentration profiles and the focus on large scale horizontal sediment gradients, we decided to use depth-averaged simulations (2DH) to speed up the simulations.

We used the third-generation short wave model SWAN (Booij, Ris, & Holthuijsen, 1999) to simulate the effect of wind-driven short waves on hydrodynamics, morphology, and transport of sand and mud through increase in bed shear stress and wave-induced momentum. This model is available within Delft3D as Delft3D-WAVE and calculates a wave field on the basis of hydrodynamic conditions and wind data. Delft3D-WAVE was coupled dynamically to Delft3D-FLOW, with the wave field being updated every hour. The effect of bottom friction in the energy balance equation in SWAN was included using the JONSWAP method described by Hasselmann, Barnett, Bouws, and Carlson (1973), and the wave-induced bed shear stress in FLOW was included using the method described by Fredsøe (1984).

Discharge time series were imposed at the two upstream (northern) open boundaries between Nieuwe Merwede and polder Spiering, and a water level time series was imposed at the downstream (southern) open boundary, discharging into Gat van de Noorderklip.

The hydrodynamic roughness was defined using Manning's friction coefficient, which was set as a uniform value for the entire area after an a priori sensitivity analysis that showed that simulated levels and flows

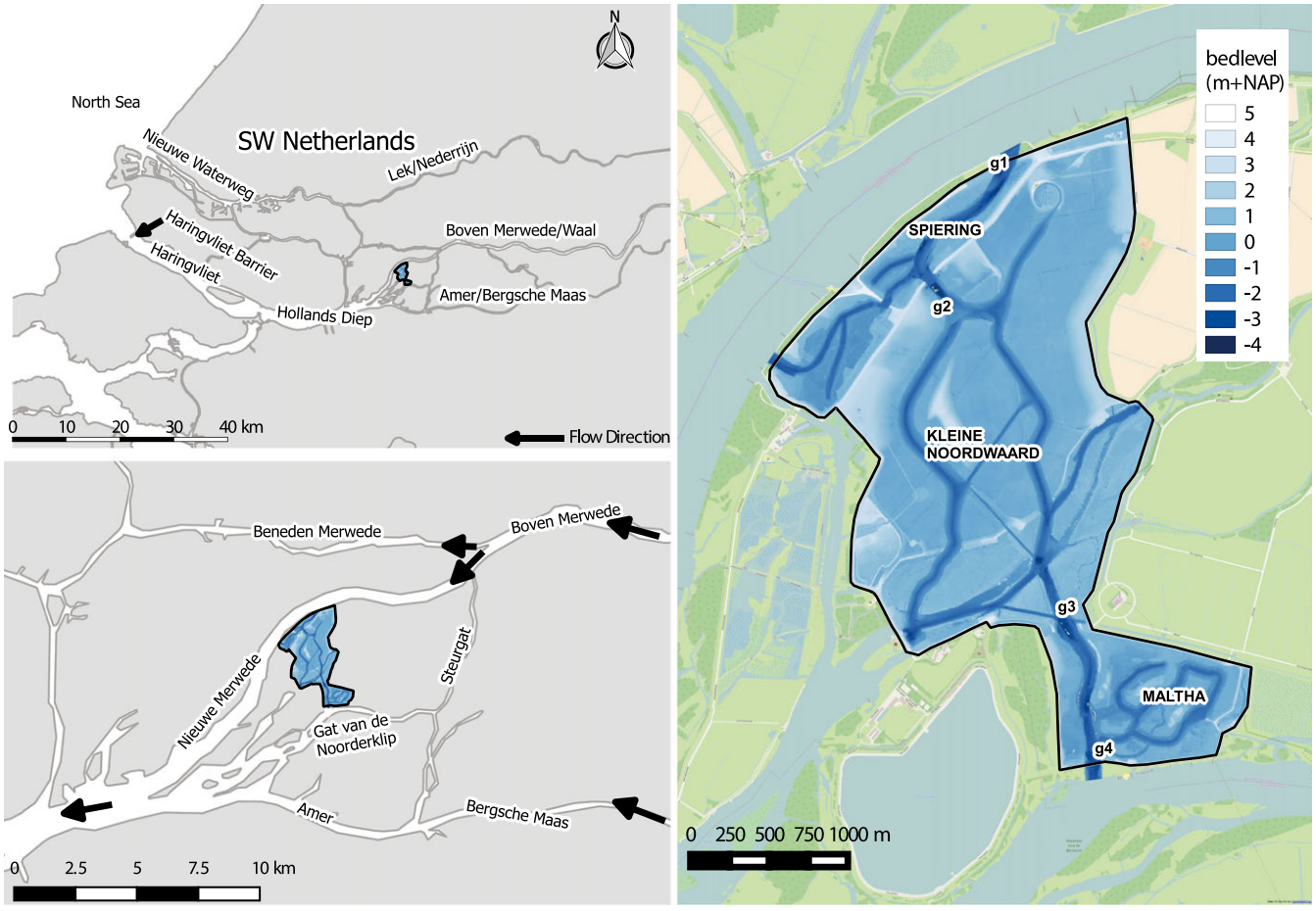

FIGURE 1 Study area. Locations g1 to g4 refer to the locations of the gauging stations in the area

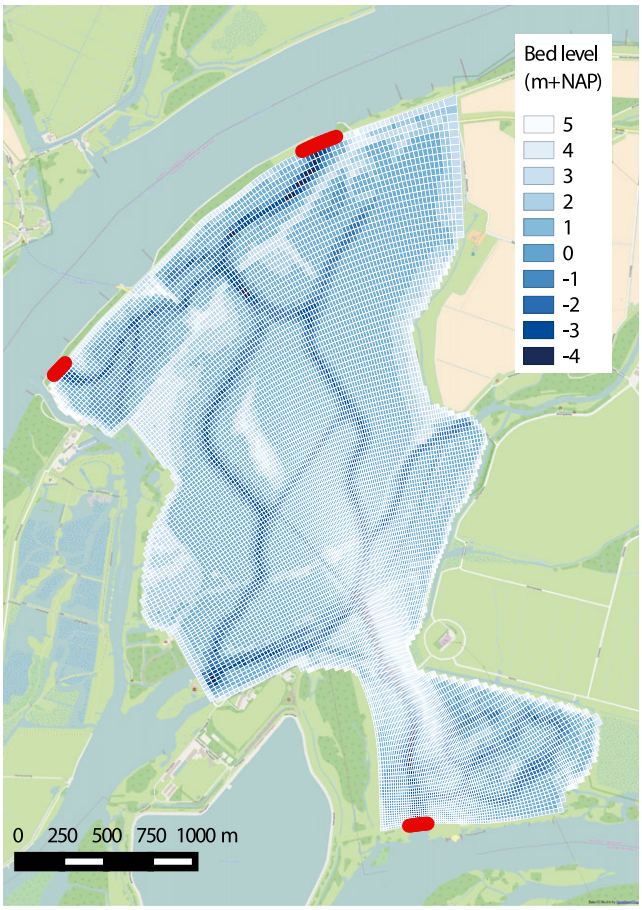

FIGURE 2 Model grid (in white), bathymetry, and open boundaries (in red)

were relatively insensitive to different patterns of distributed friction definitions due to the low flow velocities and limited amount of aquatic vegetation in this recently restored wetland. Default settings were used for all other Delft3D parameters (Deltares, 2014), except for the parameters listed in Table 1; the values for these parameters were defined on the basis of field observations and expert judgement.

3.1.3 | Sediment transport

Delft3D simulates suspended load transport of cohesive sediment fractions, suspended and bedload transport of noncohesive sediment fractions and the morphological changes that result from these processes. We defined one cohesive mud fraction and one noncohesive sand fraction. Transport of the noncohesive sediment fraction was modelled with the Van Rijn equation (Van Rijn, 1984). Uptake and settling of suspended sediment of the cohesive fraction were modelled with the Krone and Ariathurai–Partheniades formulations (Partheniades, 1965). The implementation of both transport formulae in the Delft3D framework is described by Lesser et al. (2004).

TABLE 1 Settings FLOW and SWAN models

	Unit	Value
FLOW parameter		
Horizontal eddy viscosity	m^2/s	0.5
Horizontal eddy diffusivity	m^2/s	2
Computational time step FLOW model	min	0.5
WAVE parameter		
Computational time step WAVE model	min	60
JONSWAP coefficient	m^2/s^3	0.038

To obtain input SSC at the upstream boundary of the model, we used a sediment rating curve that was constructed following a procedure described by Asselman (2000), using discharges and SSCs from station Vuren, which is the closest river gauging station along the River Waal, located 31 km upstream of the study area. The SSC values estimated with the rating curve range from 20 mg/L for average river discharge (1500 m^3/s) to 140 mg/L for extreme river discharge (6800 m^3/s). The estimated SSC values for corresponding wetland inlet discharges (between 20 and 100 m^3/s) agree well with SSCs at the inlet of the model area, which were measured using a calibrated turbidity sensor between July 2014 and April 2015.

The sediment densities of both fractions were left at default values (specific density of both mud and sand: 2650 kg/m^3; dry bed density mud: 500 kg/m^3; dry bed density sand: 1600 kg/m^3) as defined in Deltares (2013). On the basis of field observations, the effective settling velocity W_s of the mud fraction was set at 0.04 mm/s, and the D_{50} of the sand fraction at 200 μm.

The initial channel bed composition was modelled as one uniformly mixed layer with a spatially varying composition on the basis of field observations and geological maps of the area: 100% mud on the flats with a layer thickness of 2 cm, and 100% sand on the island and in the artificial channel system with a layer thickness of 3 m. The stiff polder clay layer underneath the mud layer was assumed to be non-erodible.

3.2 | Model calibration & validation

Model calibration and validation were carried out using a stepwise approach. The hydrodynamic model (including the SWAN wave module) was calibrated and validated first, subsequently, the bedload transport of the coarse fraction, and finally the suspended load transport and deposition. Because of limitations in data availability, different calibration periods were chosen for hydrodynamics and morphology.

3.2.1 | Hydrodynamic model

The hydrodynamic model was calibrated against observed water levels at three gauging stations in the case study area (points g2, g3, and g4 in Figure 1), using the root mean square error (RMSE) as optimization criterion. The Manning's roughness coefficient was used as calibration parameter with an a priori range of 0.01 to 0.05 $s/m^{1/3}$.

We selected the period between August 1, 2014 and December 1, 2014, as calibration period. August and September 2014 were relatively dry, apart from a few small discharge peaks in August. In late October 2014, there was a heavy windstorm event in combination with a small discharge peak. The calibration period ended with relatively dry and calm conditions. Discharge and water level series were derived from ADCP and diver measurements taken at the locations of the gauging stations. For more information on these time series, we refer to Van der Deijl (2015). Wind conditions (hourly values of average wind speed and direction during the last 10 min of every

hour) for four surrounding stations during the calibration period were obtained from the Royal Dutch Meteorological Institute KNMI (KNMI, 2016).

The hydrodynamic model was validated against observed water levels at the same locations for the period between December 1, 2014 and April 1, 2015. December was relatively dry and calm except for a minor discharge peak around December 23–24, 2014. In January 10–17, 2015, there was a minor combined discharge-windstorm event. The rest of the validation period was relatively dry with below-average discharges and no significant discharge peaks.

The SWAN model was not calibrated separately due to lack of quantitative data on wave characteristics. Instead, the performance was checked by comparing the significant wave heights for the calibration period with qualitative visual observations during field visits.

3.2.2 | Sediment transport model

Calibration of the sediment transport models was done at the level of 20 subareas (10 sections, see Figure 3, each further subdivided into a *channel* and a *flat* subsection), comprising the *polder Kleine Noordwaard* and *polder Maltha*. Table 2 lists the calibration parameters and their a priori value range. The specified ranges were based on a combination of available literature, expert judgement, and a priori sensitivity analysis. Calibration was carried out manually with the RMSE between measured and simulated accretion volumes (i.e., area-weighted accretion rates) in the 20 subareas over the entire calibration period as evaluation criterion.

The calibrated sediment transport model was evaluated using the Brier skill score (BSS; Sutherland, Peet, and Soulsby (2004), which is commonly used to evaluate the performance of a morphological model. We redefined the BSS in terms of bed volume changes rather than bed-level changes:

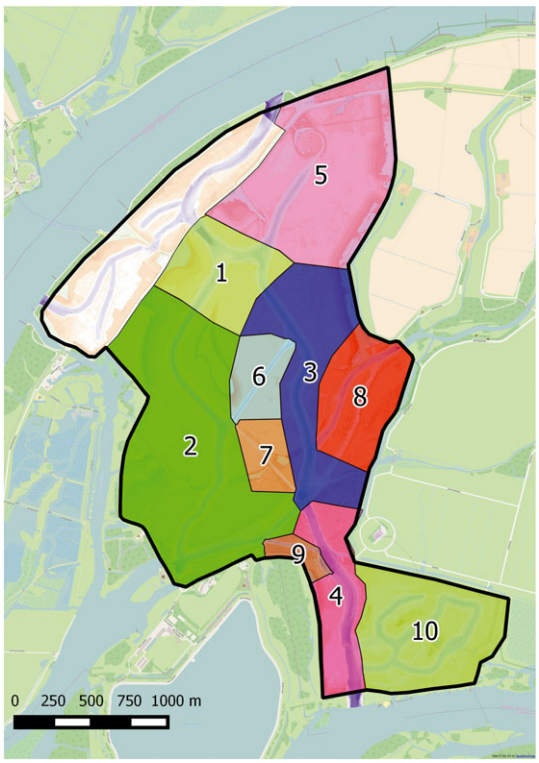

FIGURE 3 Calibration sections

TABLE 2 Sediment transport model calibration parameters and their minimum and maximum values

	Unit	Min	Max
Sand transport model parameter			
Van Rijn calibration coefficient	–	0.1	2
Roughness height	m	0.01	2
Silt transport model parameter			
Critical shear stress for sedimentation	N/m^2	0.1	2
Critical shear stress for erosion	N/m^2	0.1	2
Erosion parameter	$kg/m^2/s$	0.00001	0.1

$$BSS = 1 - \frac{\left\langle \left(\Delta V_{i,meas} - \Delta V_{i,sim}\right)^2 \right\rangle}{\left\langle \left(\Delta V_{i,sim}\right)^2 \right\rangle}. \quad (1)$$

In this equation, "⟨....⟩" denotes the arithmetic mean, in this case over the 10 * 2 subsections.

The sediment transport model was calibrated for the period between two most recent channel bathymetry surveys (March 1, 2011 to March 1, 2012). The time series of the boundary conditions for that period are shown in Figure 4. The upstream river discharge was schematized as a stepwise wave, with step values based on a cumulative frequency distribution curve for the calculated discharges (using measured water levels and flow velocities at the upstream gauging station) during the calibration period.

We used a morphological scale factor of 20 to compress the upstream discharge time series, resulting in a simulation time of almost 20 days for a 1-year period. For each computational time step, the scale factor is applied to both the erosion and deposition fluxes, thereby accelerating the bed-level changes. The use of the morphological scale factor requires that the effect of bed-level changes on hydrodynamics during one calculation time step is negligible, which can be considered valid in our study (cf. Roelvink (2006); Van der Wegen and Jaffe (2013)).

The water level series at the downstream model boundary was schematized as a harmonic wave representing the dominant wave condition (M2 tide), superimposed on a stepwise wave with values on the basis of a cumulative frequency distribution curve of the measured levels at the downstream gauging station. This method assumes a strong correlation between upstream discharge and downstream water level. For higher discharges at the inlet of the study area, this is indeed the case. However, such a strong correlation does not exist between upstream discharges and wind conditions. Therefore, we focused on wind coming from the prevailing wind direction only (SW quadrant) and constructed 10 alternative semi-random wind speed events, all of which conformed to the cumulative frequency curve for measured wind speeds. We then calculated the average morphological changes during these events and used the wind event that came closest to the average morphological changes for the calibration. We used wind data from the closest surrounding stations (hourly values, stations Cabauw, Gilze-Rijen, Herwijen, and Rotterdam) from the Dutch Meteorological Institute KNMI (KNMI, 2016) for the calibration of the sediment transport model.

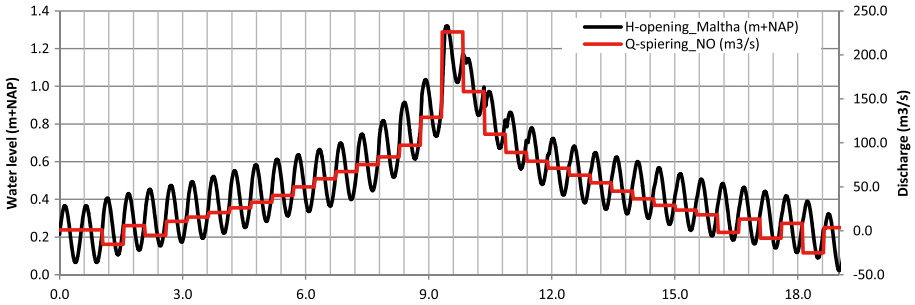

FIGURE 4 Boundary conditions for the calibration of the sediment transport model: Discharge & water level. Q = incoming discharge, H = water level at the outlet

3.3 | Sensitivity analysis

To analyse the impact of different types of hydrometeorological controls on net sedimentation quantities and patterns, a sensitivity analysis was carried out (Table 3). The analysis was carried out for the following boundary conditions:

- Discharge events of different duration and magnitudes. DISCH1 has a discharge peak with a return period of 1 year (T1) and DISCH2 a peak with a return period of 50 years (T50). Average tidal conditions (M2) apply in both cases, and there is no wind. DISCH0 is the reference scenario: a stationary discharge event without any wind and with average tidal conditions.
- Windstorm events from four different wind directions (SW, NW, NE and SE) with a return period of 1 year, with corresponding windstorm surge at sea (WIND1 through WIND4). Also one windstorm event with a return period of 50 years and SW wind direction, with corresponding windstorm surge at sea (WIND5). Average discharge conditions apply for all these events, and DISCH0 is again the reference case.
- Alternative tidal ranges: neap tide and spring tide during average discharge conditions and during a windstorm event (TIDE1 through TIDE4). WIND1 and DISCH1 are reference cases for analysing this tidal effect.
- Combinations of discharge and windstorm events: DISCH1 with WIND1 (COMB1), and DISCH1 with a smaller windstorm (with a return period of 1/25 years), both with corresponding surges at sea. WIND1 and DISCH1 are reference cases.

The event analysis was carried out as follows. First, boundary conditions for all 2D model runs were derived by using a calibrated 1D hydrodynamic model (SOBEK v.3.3) of main river channels in the entire Dutch part of the Rhine and Meuse delta (which includes a coarse model of the study area) described by (De Waal, 2007). For every hydrometeorological event, a coherent set of boundary conditions was constructed for the 1D model, on the basis of Geerse (2003) and Chbab (2012), who describe extreme value statistics of river discharge, wind conditions, and sea levels in the Rhine delta. Figure 5 shows two examples of 1D boundary conditions that were constructed on the basis of these statistics. Next, using the 1D model output as boundary

TABLE 3 Overview of event runs

	Q_lobith (m^3/s)	Wind direction	Wind speed (m/s)	Sea water level
CALIBR	N/A	Meas	Meas	N/A
DISCH0	Average (2300)	—	—	astr
DISCH1	T1 wave (5893 max)	—	—	astr
DISCH2	T50 wave (11762 max)	—	—	astr
WIND1	Average (2300)	SW	T1 (17.9)	astr + surge
WIND2	Average (2300)	NW	T1 (14.4)	astr + surge
WIND3	Average (2300)	NE	T1 (11.8)	astr + surge
WIND4	Average (2300)	SE	T1 (9.3)	astr + surge
TIDE1	Average (2300)	SW	T1 (17.9)	astr + surge + NT
TIDE2	Average (2300)	SW	T1 (17.9)	astr + surge + ST
TIDE3	T1 wave (5893 max)	—	—	astr + NT
TIDE4	T1 wave (5893 max)	—	—	astr + ST
COMB1	T1 wave (5893 max)	SW	T1 (17.9)	astr + surge
COMB2	T1 wave (5893 max)	SW	T(1/25; 6.4)	astr + surge
WIND5	Average (2300)	SW	T50 (24.3)	astr + surge

Note. Q_lobith and sea water level refer to the upstream discharge and downstream water level boundary of the 1D model of the Dutch part of the Rhine delta. T1, T50, and T(1/25) refer to the return periods of the events (1, 50, and 0.04 years, respectively). Note that the magnitude of the T1 wind speed is different for every direction, and that SW winds are most common.

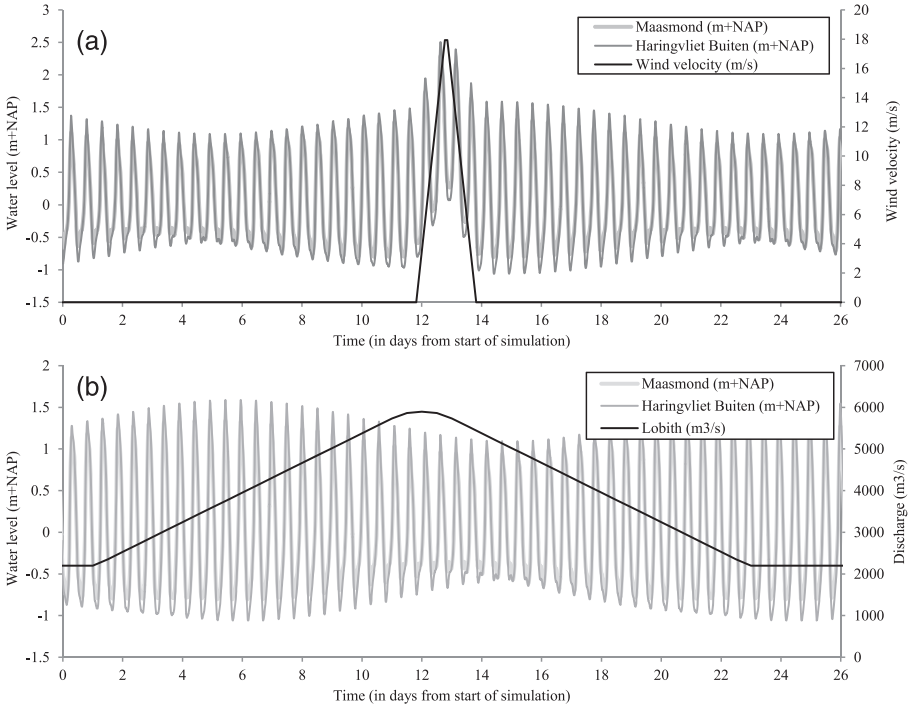

FIGURE 5 1D model boundary conditions for runs TIDE2 (a) and TIDE3 (b). Lobith refers to the location of the upstream boundary, and Maasmond and Haringvliet Buiten are the locations of the downstream boundaries of the 1D model (at the mouths of Nieuwe Waterweg and Haringvliet, respectively, see Figure 1). In (a), the discharge boundary Q (location Lobith) has a constant value of 2300 m^3/s and is purposefully omitted. In (b), the wind velocity has a constant value of 0 m/s for this run and is purposefully omitted

conditions, every event was simulated with the 2D model to simulate corresponding water flow, sedimentation quantities, and patterns within the study area. All events had the same simulation period of 26 days (even though windstorm events only last 48 hr) in order to make the results comparable.

4 | RESULTS

4.1 | Calibration and validation

4.1.1 | Hydrodynamic model

The calibration of the hydrodynamic model yielded a best fit when Manning's roughness coefficient was set at 0.025 $s/m^{1/3}$. Figure 6 shows the observed and simulated water levels using the calibrated model for the inlet of the Kleine Noordwaard (measurement location G2). Table 4 summarizes the model performance criteria for the three measurement locations. It can be concluded that the calibration of the hydrodynamic model resulted in a good agreement between the observed and simulated water levels for both the calibration and validation period.

4.1.2 | Sediment transport model

The results of the manual calibration of the sediment transport model are summarized in Figure 7. This chart shows the measured and simulated cumulative sedimentation and erosion volumes in the model area during the calibration period. The associated (lowest) RMSE is 1.3×10^3 m^3. The results in most sections agree reasonably well with the measurements except for section 10 (Figure 3), for which the model overestimated erosion in the channels and underestimated sedimentation on the flats.

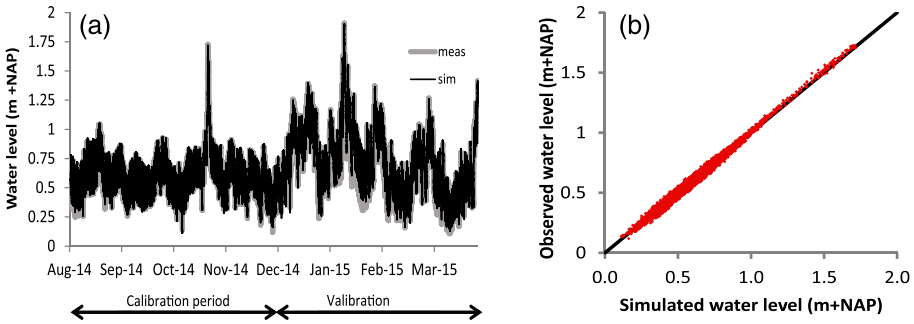

FIGURE 6 (a) simulated and observed water levels for entire calibration-validation period at station G2. (b) scatter plot of observed water levels against simulated water levels at station G2 for the calibration period

TABLE 4 Model performance indicators for the calibrated model

	Calibration period			Validation period		
Location	ME (cm)	RMSE (cm)	NSE (−)	ME (cm)	RMSE (cm)	NSE (−)
(G1) Opening Spiering	−0.19	1.80	0.99	−1.25	2.91	0.99
(G2) Brug Bandijk	−1.97	2.41	0.98	−2.47	3.24	0.99
(G3) Brug Maltha	−0.09	0.46	1.00	0.71	0.88	1.00

Note. ME = mean error (cm); RMSE = root mean square error (cm); NSE = Nash–Sutcliffe efficiency index (−).

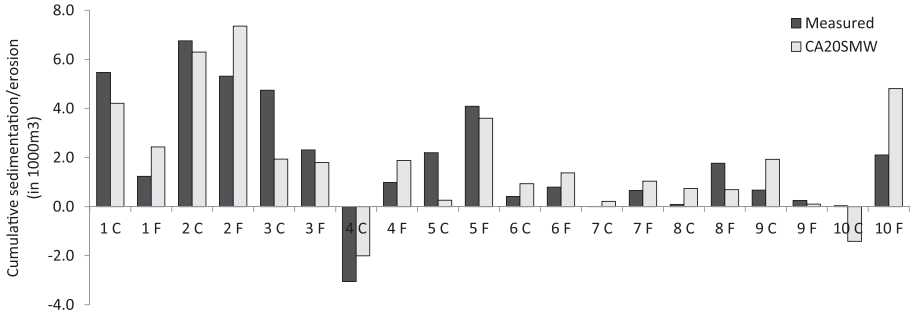

FIGURE 7 Cumulative sedimentation/erosion (in 1000 m^3) per subsection (numbered 1 to 10) over the calibration period. "C" stands for "channel," "F" for "flat". Note that the measured values for the flats are based on the estimation of a uniform accretion rate of 0.5 cm per year

The resulting set of calibrated parameter values is listed in Table 5. The evaluation criterion BSS equals 0.81, which means that the performance of the morphological model can be classified as "good" according to the Sutherland's proposed classification table (Sutherland et al., 2004).

4.2 | Sensitivity to varying boundary conditions

4.2.1 | Discharge events

High shear stresses occurring at the inflow point in the northern part of the study area (Polder Spiering) cause sand on the channel bed to move in downstream direction, towards the major bifurcation in Polder Noordwaard, where the sand is deposited on the bar in-between the bifurcating channels (Figure 8). Close to the outlet of the system (between g3 and g4 in Figure 1), the high shear stresses in the converging water flow cause the channel bed material to become mobilized and to leave the area both through bedload and suspended transport. Thus, close to the inlet, mostly an internal redistribution of sand occurs, whereas close to the outlet, there is a net loss of sand from the area. In the channel system, further away from the in- and outlet shear stresses are too low for mobilizing or transporting sand, leading to stable channels. Overall, bed-level changes in the channel system are dominated by deposition and erosion of sand and exhibit a strong correlation with the magnitude of the discharge event (Figure 9).

Sedimentation of mud on the flats mostly takes place close to the channels due the large gradient in flow velocity there (Figure 9). However, higher discharges deposit the material farther away from the channels due to the larger water depth and consequent smaller gradient in flow velocities. Local topographic irregularities in the bottom surface also affect the deposition patterns: The former drainage ditches prove to be very good sediment traps, and former roads or small dikes may prevent sediment loaded water from flowing back to the channels after the highest water levels have passed. This is especially notable for the heaviest discharge event, which inundates the entire system. Gradual sediment depletion causes a small gradient in sediment deposition from the inlet (more sedimentation) to the outlet (less sedimentation). Deposition of the mud inside the channels occurs only to a very small extent: mainly in the dead-end channels on the eastern side of the system.

Larger discharges cause both more erosion of mud in the channels and more sedimentation on the flats (Figure 9). There is no direct relation between these two effects: The bed level of the flats increases mostly because of sedimentation of silts coming from the upstream boundary, whereas the sand that erodes from the channels stays in suspension and leaves the area through the downstream boundary. Sedimentation of suspended sand occurs only on a specific part of the flats close to the post-confluence channel section.

The total amount of mud retained in the study area increases with the magnitude of the discharge peak and corresponding increased influx of sediment whereas the mud trapping efficiency decreases (Figure 10). The reduced trapping efficiency is caused by the increased shear stresses during the high-discharge events, which also causes most of the fines to stay in suspension during their transport through the channels in the area.

TABLE 5 Parameter settings of calibrated sediment transport model

	Unit	Value
Sand transport model parameter		
Van Rijn calibration coefficient	—	1.5
Roughness height (m)	m	0.4
Silt transport model parameter		
Critical shear stress for sedimentation	N/m2	0.1
Critical shear stress for erosion	N/m2	0.3
Erosion parameter	kg/m2/s	0.001

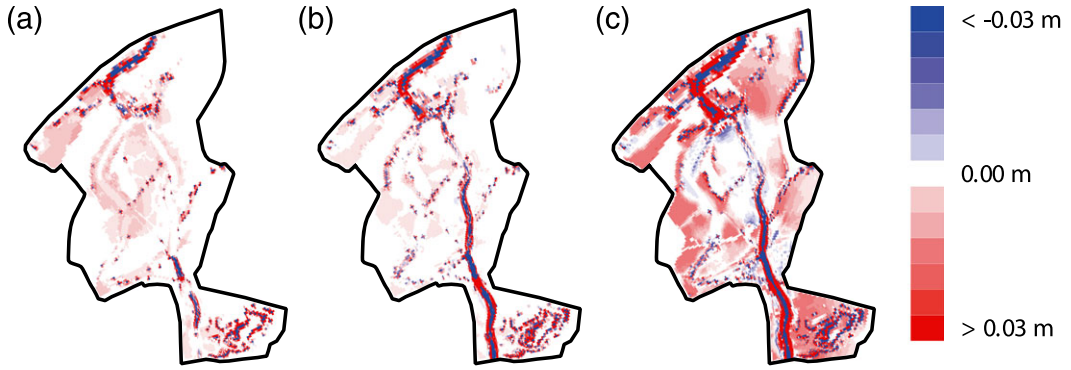

FIGURE 8 Impact of discharge events on erosion/sedimentation patterns compared to the reference case. (a) sedimentation/ erosion pattern of the reference case DISCH0, (b) and (c) sedimentation/erosion pattern of DISCH1 and DISCH2 minus the sedimentation/erosion pattern of DISCH0, respectively

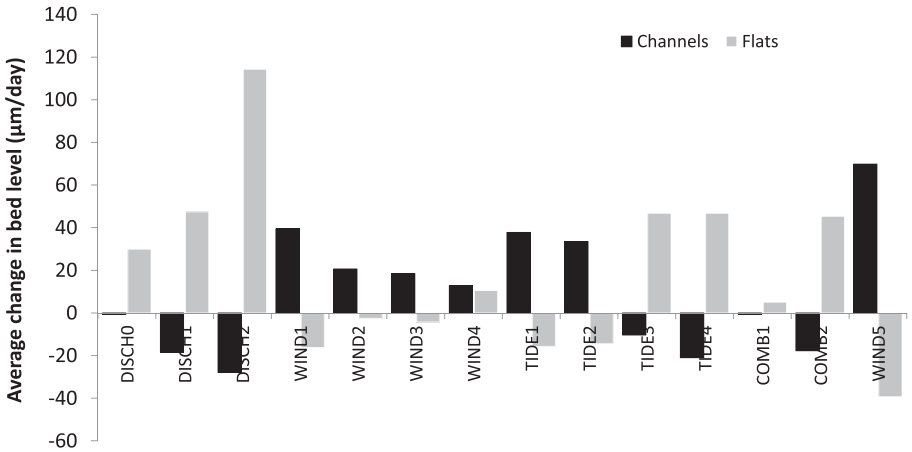

FIGURE 9 Change in average bed level of the channels and flats for all event runs

4.2.2 | Windstorm events

The analysed windstorms have a large impact on the net sedimentation/erosion patterns compared to the reference case: All storm scenarios lead to less sedimentation on the flats (Figure 11) through resuspension of fine sediment. This is the result of a combination of a relatively shallow water depth and large fetch length, which leads to the development of wind waves that can reach the bed level and hence cause bed shear stresses to increase. Part of the resuspended sediment settles in the deeper channel system due to the low shear stresses resulting from the stable, stationary discharge conditions. This causes correlation between the decrease of the average bed level of the flats and the increase of average bed level inside the channel (Figure 9).

Another part of the mobilized mud is redistributed over the flats, with sedimentation/erosion patterns largely governed by the wind direction: Most of the sedimentation occurs on the lee side of the island, and erosion takes place especially in those areas where the waves are most developed (Figure 11). In WIND1 for example, the relatively long fetches in the NE part of the system caused most of the erosion to take place in that particular area. In WIND2 on the other hand, the geometry of the SE part of the area (Polder Maltha) restricted the build-up of significant waves during the event, leading to less erosion.

The rest of the resuspended mud stays mobile and leaves the study area through the downstream outlet with the stationary water discharge. This leads to a net reduction in mud trapping efficiency for all windstorm events, regardless magnitude and direction, when compared to the reference case DISCH0 without wind (Figures 10 and 12). The only exception is WIND4. This event has the lowest wind speed of all T1 windstorm events as well as a wind direction that is opposite to the flow direction, which causes it to have a less pronounced impact on the mud trapping efficiency than the other T1 windstorm events (Figure 11).

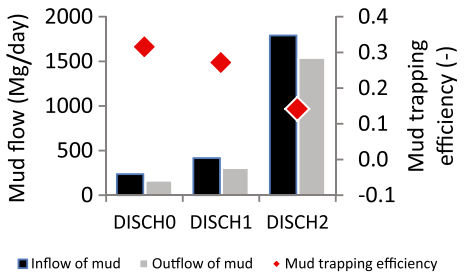

FIGURE 10 Average daily inflow and outflow of mud, and the fraction of mud retained in the study area (trapping efficiency) for increasing discharge magnitudes (DISCH1 and DISCH2). DISCH0 is the case with a (yearly average) stationary discharge and is included for reference

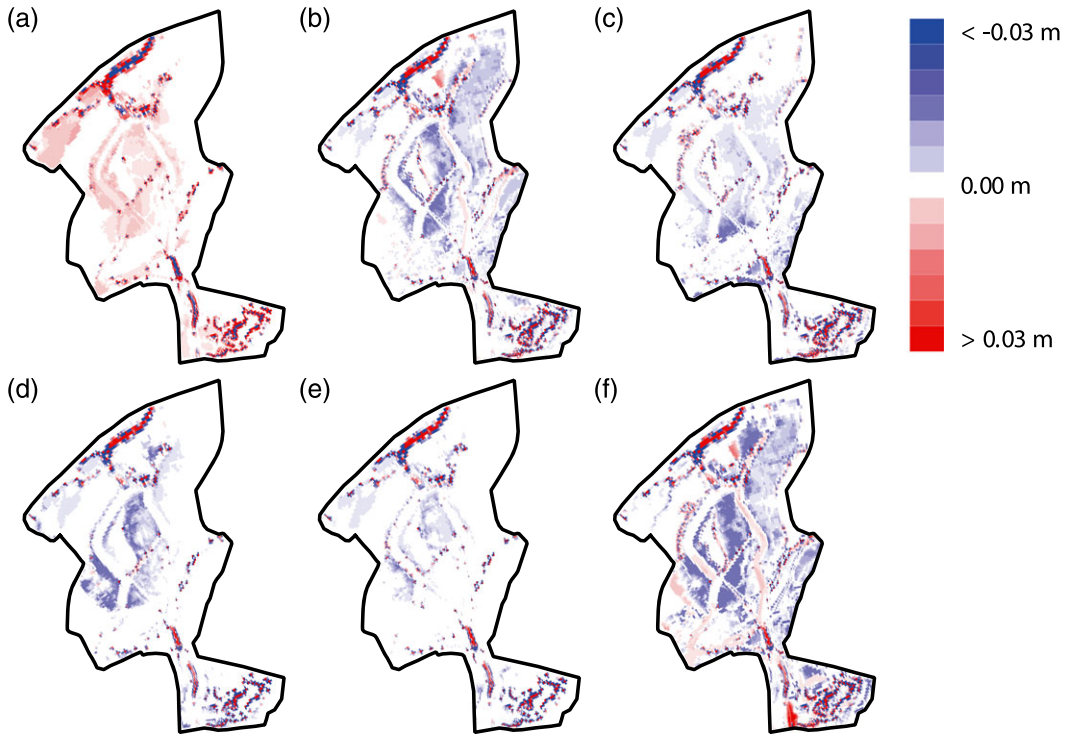

FIGURE 11 Impact of windstorm events on erosion/sedimentation patterns compared to the reference case. (a) sedimentation/erosion pattern of the reference case DISCH0. (b) sedimentation/erosion pattern of WIND1 minus the sedimentation/erosion pattern of DISCH0. (c) through (f) corresponding differences with the reference case of WIND2 through WIND5

WIND5 is the only event that leads to an outflow of sediment that is larger than the sediment inflow and hence results in a negative trapping efficiency (Figure 12). The T50 SW storm causes wave heights on the flats of up to 25 cm, preventing new sediment from settling and bringing most of the existing sediment into suspension. This also results in this event having the largest decrease in bed levels of the flats of all events (Figure 9). Furthermore, WIND5 is the only event that leads to a net accumulation of sand in the study area. This is caused by the strong SW wind during the periods of reversed flow direction in the southern part of the study area, which fills an area close to the outlet (Polder Maltha) with sand in suspension from the northern section of the study area, where the flow direction is not reversed. Although this process may indeed occur in reality, we did not have sufficient data to verify this model outcome. Finally, WIND5 also causes the largest increase in bed level in the channels of all events (Figure 9). Most of this increase can however be attributed to the deposition of sand in polder Maltha.

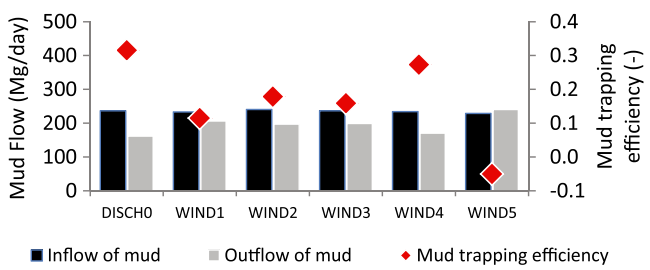

FIGURE 12 Average daily inflow and outflow of mud, and the fraction of mud retained in the study area (trapping efficiency) for alternative WIND directions (WIND1 to WIND4) and magnitude (WIND5) DISCH0 is included for reference

4.2.3 | Tidal range

Varying the tidal range from average to neap or spring tide has little effect on the sedimentation/erosion patterns compared to both reference cases (Figure 13), even though these patterns seem to be strongly affected by tidal water level fluctuations. The net retention rates of mud compared to both reference cases remain also relatively unaffected (Figure 14). Still, the net outflow of sand from the study area during the discharge event depends slightly on the tidal amplitude, with a decrease during neap tide (TIDE3) and an increase during spring tide (TIDE4; Annex). The average channel bed level changes accordingly (Figure 9).

4.2.4 | Combined discharge – Windstorm events

A T1 windstorm coinciding with a discharge event (COMB1) mobilizes the initial mud layer on the flats in a similar fashion as during average discharge conditions (e.g., WIND1), albeit to a slightly lesser extent. This is the result of the increased water depth in the system due to the discharge event, which makes it more difficult for the wind waves to reach the bed. The wind also hinders the settling on the flats of "new" sediment entering the system with the discharge wave, which results in a negligible increase of average bed level of the flats (Figure 9). Part of the resuspended sediment settles in the deeper parts of channel system which, in combination with the bed erosion occurring in other parts during the passing of the discharge event, leads to an almost neutral channel bed level change (Figure 9).

Another part of the mobilized mud is redistributed over the flats. The sedimentation/erosion pattern of COMB1 strongly resembles WIND1 (Figure 15), although the total amount of sedimentation on

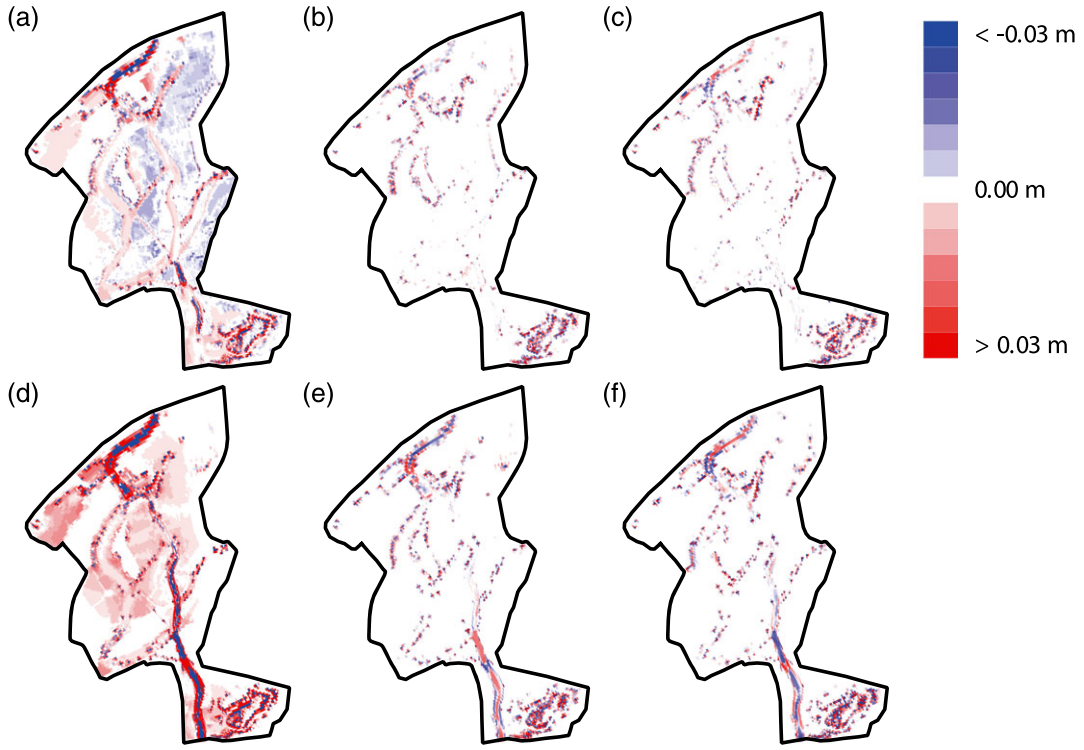

FIGURE 13 Impact of tidal range on erosion/sedimentation patterns compared to two reference cases. (a) shows the sedimentation/erosion pattern of reference case WIND1. (b and c) sedimentation/erosion pattern of TIDE1 and TIDE2 minus the sedimentation/erosion pattern of (a), respectively. (d) Sedimentation/erosion pattern of reference case DISCH1. (e and f) Sedimentation/erosion pattern of TIDE3 resp TIDE4 minus the sedimentation/ erosion pattern of (d), respectively

the flats is slightly higher in the combined case because of the passing of a discharge wave.

The rest of the resuspended mud remains mobile and leaves the study area through the downstream outlet, together with the sediment that originates from the upstream boundary and that was unable to settle on the flats due to the wind conditions. This leads to a large reduction in mud trapping efficiency when compared to reference case DISCH1 (Figure 16). A much smaller windstorm (COMB2) still leads to a reduction of sediment trapping efficiency compared to the base case DISCH1, albeit very small.

Trapping efficiencies of combined discharge-windstorm events depend on both parameters as follows: Given an average discharge regime, switching from a T1 windstorm to a T50 windstorm leads to a large reduction in trapping efficiency (Figure 17). Given a T50 discharge event however, the trapping efficiency is reduced by only a small amount when switching from a T1 to T50 windstorm. We hypothesize that the larger water depths during the T50 discharge event reduce the impact of the waves on the bed shear stresses, thereby effectively reducing the resuspension of mud. Furthermore, increased sedimentation occurs in those areas that are less affected by wind, such as the deep dead-end channel sections and parts on the lee side of the island.

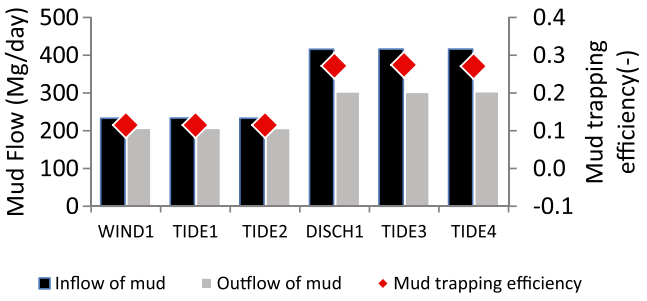

FIGURE 14 Average daily inflow and outflow of mud, and the fraction of mud retained in the study area (trapping efficiency) for cases with alternative tidal range (neap and spring) during a windstorm event (TIDE1 and TIDE2) and during a discharge event (TIDE3 and TIDE4). WIND1 and DISCH1 are included for reference

5 | DISCUSSION

Our site-specific results show the sedimentation patterns and rates inside a flow-through TFW, and how these change in response to various combinations of hydrometeorological controls. Until now, most research focused on a single control on sedimentation processes in a wetland (e.g., Mariotti & Fagherazzi, 2013; Temmerman et al., 2003b); however, our results demonstrate that there are cases in which there is important interaction among the three controls (discharge, wind, and tide). In this section, we discuss the role of both separate and combined controls, first on the sediment balance and trapping efficiency and then on sedimentation patterns.

For our study area, the role of the separate controls on the *sediment balance terms* and the *sediment trapping efficiency* is as follows: River input is the major source of sediment of this flow-through wetland, and the discharge through the inlet determines net sediment deposition rates (positive correlation, due to increased amounts of

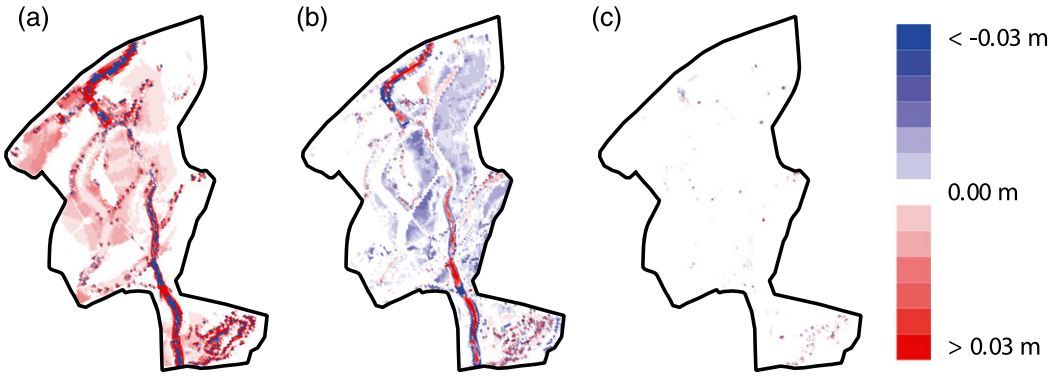

FIGURE 15 Impact of combined discharge-windstorm events on erosion/sedimentation patterns compared to the reference case. (a) sedimentation/erosion pattern of the reference case DISCH1. (b) and (c) sedimentation/erosion pattern of COMB1 resp COMB2 minus the sedimentation/erosion pattern of DISCH1

sediment conveyed into the area) and trapping efficiency (negative correlation due to increased bed shear stresses at higher flow velocities). Similar relations were reported by for example Yang et al. (2005), who linked reduction in vertical growth rate of intertidal wetlands in the Yangtze delta to decreased riverine sediment supply caused by the construction of a large number of dams. Wind causes resuspension of fine sediments, similar to the processes taking place in shallow lakes such as Lake Markermeer, the Netherlands (Kelderman, Ang'weya, De Rozari, & Vijverberg, 2011). A large part of the resuspended material immediately leaves the area along with the continuous water flow through the wetland. This causes the trapping efficiency to decrease for increasing wind speeds. Varying tidal range (neap and spring) has surprisingly little effect on the sediment balance, although the wetland is located in the backwater of the sea. This low impact is largely caused by the presence of a saltwater barrier (Haringvliet sluices) downstream of the wetland, which severely dampens the tidal signal. In other TFWs tidal range was shown to be a major control of sedimentation (e.g., Kirwan & Guntenspergen, 2010; Vandenbruwaene et al., 2011) and should therefore normally not be neglected.

The combined impact of discharge and wind on the sediment balance and trapping efficiency is as follows: With increasing discharge, the impact of wind through resuspension decreases due to the increased water depths caused by higher discharges along with wind set-up on the Haringvliet estuary (for westerly wind). Net loss of sediment from the area only occurs during extreme windstorms in combination with low flow-through discharges—all other combinations lead to a positive trapping efficiency, albeit very small for cases with wind and low discharges.

With respect to *sedimentation patterns* in the study area, our results generally agree with previous research in similar areas (e.g., Delgado et al., 2013; Hupp et al., 2008; Mitsch et al., 2014; Temmerman et al., 2003b): The highest sedimentation rates are found close to the inlet of the wetland and close to the internal channel network. Topographic irregularities in the submerged terrain—particularly former polder drainage ditches and old embankments—also influence local sedimentation patterns. Larger discharge events cause a larger portion of the sediment to settle farther away from the inlet and the channels. Wind influences sedimentation patterns by resuspension and internal redistribution, usually resulting in a net transport of sediment from the flats towards the channels.

The impact of wind on bed shear stresses is caused especially by locally generated wind waves and not by wind-driven currents. This is also observed in tidal mudflats, for example, along the Westerscheldt estuary (Callaghan et al., 2010). Interestingly, we find an almost linear

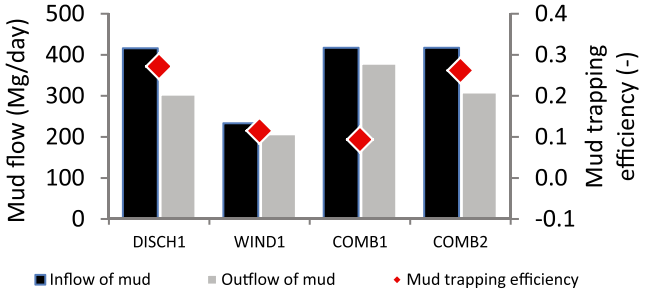

FIGURE 16 Average daily inflow and outflow of mud, and the fraction of mud retained in the study area (trapping efficiency) for combined discharge-windstorm events COMB1 and COMB2. DISCH1 and WIND1 are included for reference

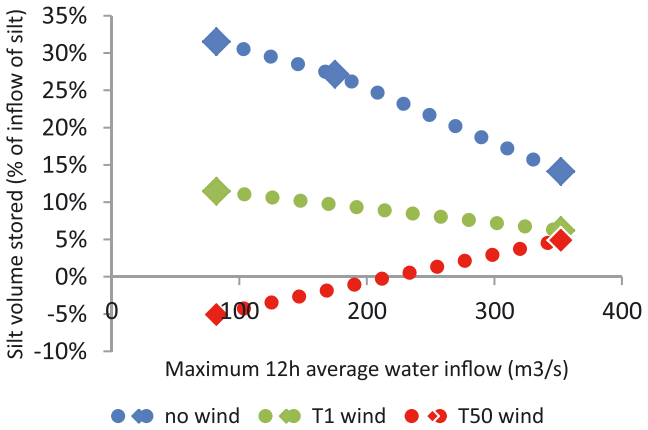

FIGURE 17 Relation between discharge magnitude (defined by the maximum 12-hr moving average water inflow from the upstream boundary) and sediment trapping efficiency for three different windstorm scenarios (all from SW). The discharge values of 82, 175, and 352 m^3/s correspond to average discharge, T1 and T50 discharge, respectively

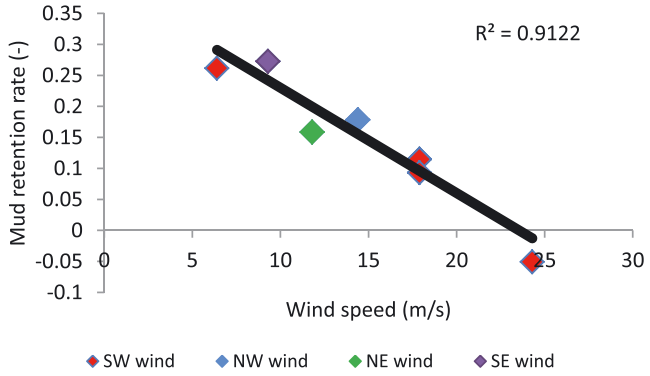

FIGURE 18 Relation between wind speed and mud retention rate

(negative) correlation between wind speed and mud retention, for all wind directions (Figure 18), even though fetch lengths for the various wind directions show large differences due to the distinctly elongated shape of the study area along the NW–SE axis. As Mariotti and Fagherazzi (2013) pointed out for the case of a tidal mud flat in Willapa Bay, USA, different fetches only start to impact bed shear stress above a certain critical water depth. We hypothesize that water depths in our study area (generally between 0.1 and 1 m) are below this critical value. The determination of this critical depth is an interesting topic for further research.

To answer the question whether this TFW will survive the impact of SLR, the next step will be to analyse long-term effects for different climate scenarios in which the frequency and duration of these and other events are incorporated in longer time series and are adapted in accordance with future climate scenarios. This step also requires that the effect of vegetation and possibly subsidence be accounted for in the models. Application to other TFWs in the world requires further extension of the analysis by evaluating the effects on sedimentation rates and patterns of for example wetland size, shape, position within the delta (distance to turbidity maximum), and vegetation.

6 | CONCLUSIONS

To gain insight in both the average wetland surface accretion rates and the spatial sediment distribution in a TFW and the role of various different controls, we developed a combined hydrodynamic, morphological and wave model of a TFW in the Netherlands and applied it to analyse sediment rates and patterns for various windstorm and discharge events under different tidal conditions. The main conclusions for this area are as follows:

- The net sediment deposition rate inside the TFW increases with water discharge magnitude and associated increases in SSC of the inflowing water, decreases with windstorm magnitude, and is relatively unaffected by changes in tidal conditions (neap and spring).
- The trapping efficiency decreases with water discharge magnitude as a result of increased bed shear stresses. Windstorms during any discharge event reduce the trapping efficiency compared to the same discharge event without any wind. The actual reduction increases with wind velocity, depends on wind direction (highest for SW winds), and decreases for higher water inflow from the river.
- Sedimentation rates are highest close to the inlet of the wetland, and the channel system within the wetland. Local sedimentation patterns are affected by irregularities in the topography, particularly former polder drainage channels and old embankments.
- Regardless of wind direction, windstorms lead to (a) a net transport of sediment from the flats towards the channels, (b) a net transport from the downwind sections of the flats to other sections, and (c) an increased outflow of sediment from the study area.
- TFWs have the potential to trap large amounts of sediment, yet the actual deposition rate shows large variations depending on the interplay between discharge conditions, windstorms and tidal conditions. This interplay should be taken into account when predicting long-term sedimentation rates.

Results are found to be in line with findings from previous studies. However, the specific location of this wetland in-between tidally and fluvially dominated areas makes it particularly important to consider the various controls or boundary conditions in combination. Follow-up research will focus on (a) the identification of critical thresholds of combined boundary conditions for sedimentation and erosion in TFWs and (b) the application of the model to quantify the long-term response of the TFW to SLR.

ACKNOWLEDGMENTS

This study was financed by the Dutch Technology Foundation STW (project no. 12431). We thank everybody who assisted us with the data collection, especially Dr. H. de Boois. We thank the people of Staatsbosbeheer and Rijkwaterstaat-WNZ for the provided data, logistic support, and assistance. We also thank two anonymous referees for their careful reviews and constructive comments.

REFERENCES

Anderson, C. J., & Lockaby, B. G. (2012). Seasonal patterns of river connectivity and saltwater intrusion in tidal freshwater forested wetlands. *River Research and Applications*, *28*, 814–826. https://doi.org/10.1002/rra.1489

Asselman, N. E. M. (2000). Fitting and interpretation of sediment rating curves. *Journal of Hydrology*, *234*, 228–248. https://doi.org/10.1016/S0022-1694(00)00253-5

Asselman, N. E. M., Middelkoop, H., & van Dijk, P. M. (2003). The impact of changes in climate and land use on soil erosion, transport and deposition of suspended sediment in the river Rhine. *Hydrological Processes*, *17*, 3225–3244. https://doi.org/10.1002/hyp.1384

Booij, N., Ris, R. C., & Holthuijsen, L. H. (1999). A third-generation wave model for coastal regions: 1. Model description and validation. *Journal of Geophysical Research: Oceans*, *104*, 7649–7666. https://doi.org/10.1029/98JC02622

Brueske, C. C., & Barrett, G. W. (1994). Effects of vegetation and hydrologic load on sedimentation patterns in experimental wetland ecosystems. *Ecological Engineering*, *3*, 429–447. https://doi.org/10.1016/0925-8574(94)00011-5

Burkett, V., & Kusler, J. (2000). Climate change: Potential impacts and interactions in wetlands of the United States. *JAWRA Journal of the American Water Resources Association*, *36*, 313–320. https://doi.org/10.1111/j.1752-1688.2000.tb04270.x

Callaghan, D. P., Bouma, T. J., Klaassen, P., van der Wal, D., Stive, M. J. F., & Herman, P. M. J. (2010). Hydrodynamic forcing on salt-marsh development: Distinguishing the relative importance of waves and tidal flows. *Estuarine, Coastal and Shelf Science*, *89*, 73–88. https://doi.org/10.1016/j.ecss.2010.05.013

Chbab, H. (2012). Achtergrondrapportage hydraulische belasting voor de Benedenrivieren. Deltares rapport 1204143–003.

Darke, A. K., & Megonigal, J. P. (2003). Control of sediment deposition rates in two mid-Atlantic Coast tidal freshwater wetlands. *Estuarine, Coastal and Shelf Science*, *57*, 255–268. https://doi.org/10.1016/s0272-7714(02)00353-0.

De Waal, J. P. (2007). Achtergrondrapport HR 2006 voor de Benedenrivieren. Thermometerrandvoorwaarden 2006. RWS RIZA rapport 2007.023. ISBN 978–90–369-1402-4.

Delgado, P., Hensel, P. F., Swarth, C. W., Ceroni, M., & Boumans, R. (2013). Sustainability of a tidal freshwater marsh exposed to a long-term hydrologic barrier and sea level rise. *Estuaries and Coasts*, *36*, 585–594. https://doi.org/10.1007/s12237-013-9587-2

Deltares. (2013). Delft3D-FLOW User Manual. Version: 3.15.30932 -: -.

Deltares. (2014). Delft3D-WAVE simulation of short-crested waves with SWAN. User Manual. Version: 3.05.34160. 28 May 2014.

Fredsøe, J. (1984). Turbulent boundary layer in wave-current motion. *Journal of Hydraulic Engineering*, *110*, 1103–1120. https://doi.org/10.1061/(asce)0733-9429(1984)110:8(1103)

Geerse, C. P. M. (2003). Probabilistisch model hydraulische randvoorwaarden Benedenrivierengebied. RWS RIZA werkdocument 2003.128x.

Hasselmann, K., Barnett, T. P., Bouws, E., & Carlson, H. (1973). Measurements of wind-wave growth and swell decay during the Joint North Sea Wave Project (JONSWAP). Deutsche hydrographische Zeitschrift Reihe A, Nr.12, Ergänzungsheft:

Hupp, C. R., & Bazemore, D. E. (1993). Introduction to the 28th International Geological Congress Symposium on the Hydrogeology of Wetlands: Temporal and spatial patterns of wetland sedimentation, West Tennessee. *Journal of Hydrology*, *141*, 179–196. https://doi.org/10.1016/0022-1694(93)90049-F

Hupp, C., Demas, C., Kroes, D., Day, R., & Doyle, T. (2008). Recent sedimentation patterns within the central Atchafalaya Basin, Louisiana. *Wetlands*, *28*, 125–140. https://doi.org/10.1672/06-132.1

Kelderman, P., Ang'weya, R. O., De Rozari, P., & Vijverberg, T. (2011). Sediment characteristics and wind-induced sediment dynamics in shallow Lake Markermeer, the Netherlands. *Aquatic Sciences*, *74*, 301–313. https://doi.org/10.1007/s00027-011-0222-7

Kirwan, M. L., & Guntenspergen, G. R. (2010). Influence of tidal range on the stability of coastal marshland. *Journal of Geophysical Research: Earth Surface*, *115*, n/a–n/a. https://doi.org/10.1029/2009JF001400

Kirwan, M. L., & Megonigal, J. P. (2013). Tidal wetland stability in the face of human impacts and sea-level rise. *Nature*, *504*, 53–60. https://doi.org/10.1038/nature12856

Kleinhans, M. G., Weerts, H. J. T., & Cohen, K. M. (2010). Avulsion in action: Reconstruction and modelling sedimentation pace and upstream flood water levels following a Medieval tidal-river diversion catastrophe (Biesbosch, The Netherlands, 1421–1750AD). *Geomorphology*, *118*, 65–79. https://doi.org/10.1016/j.geomorph.2009.12.009

KNMI. (2016). Uurgegevens van het weer in Nederland. http://www.knmi.nl/nederlandnu/klimatologie/uurgegevens. Downloaded at 4 february 2016.

Leonardi, N., Kolker, A. S., & Fagherazzi, S. (2015). Interplay between river discharge and tides in a delta distributary. *Advances in Water Resources*, *80*, 69–78. https://doi.org/10.1016/j.advwatres.2015.03.005

Lesser, G. R., Roelvink, J. A., van Kester, J. A. T. M., & Stelling, G. S. (2004). Development and validation of a three-dimensional morphological model. *Coastal Engineering*, *51*, 883–915. https://doi.org/10.1016/j.coastaleng.2004.07.014

Mariotti, G., & Fagherazzi, S. (2013). Wind waves on a mudflat: The influence of fetch and depth on bed shear stresses. *Continental Shelf Research*, *60* (Supplement), S99–S110. https://doi.org/10.1016/j.csr.2012.03.001

Millennium Ecosystem Assessment. (2005). Ecosystems and human well-being: Wetlands and water synthesis. World Resources Institute: Washington, DC.

Mitsch, W. J., Nedrich, S. M., Harter, S. K., Anderson, C., Nahlik, A. M., & Bernal, B. (2014). Sedimentation in created freshwater riverine wetlands: 15 Years of succession and contrast of methods. *Ecological Engineering*, *72*, 25–34. https://doi.org/10.1016/j.ecoleng.2014.09.116

Nardin, W., & Edmonds, D. A. (2014). Optimum vegetation height and density for inorganic sedimentation in deltaic marshes. *Nature Geoscience*, *7*, 722–726. https://doi.org/10.1038/ngeo2233

Nardin, W., Edmonds, D. A., & Fagherazzi, S. (2016). Influence of vegetation on spatial patterns of sediment deposition in deltaic islands during flood. *Advances in Water Resources*, *93*, *Part B*, 236–248. https://doi.org/10.1016/j.advwatres.2016.01.001

Neubauer, S. C., Anderson, I. C., Constantine, J. A., & Kuehl, S. A. (2002). Sediment deposition and accretion in a mid-Atlantic (U.S.A.) tidal freshwater marsh. Estuarine. *Coastal and Shelf Science*, *54*, 713–727. https://doi.org/10.1006/ecss.2001.0854

Orson, R. A., Simpson, R. L., & Good, R. E. (1990). Rates of sediment accumulation in a tidal freshwater marsh. *Journal of Sedimentary Research*, *60*, 859–869.

Paola, C., Twilley, R. R., Edmonds, D. A., Kim, W., Mohrig, D., Parker, G., … Voller, V. R. (2011). Natural processes in delta restoration: Application to the Mississippi Delta. *Annual Review of Marine Science*, *3*, 67–91. https://doi.org/10.1146/annurev-marine-120709-142856

Partheniades, E. (1965). Erosion and deposition of cohesive soils. *Journal of the Hydraulics Division*, *91*, 105–139.

Pasternack, G. B., & Brush, G. S. (2001). Seasonal variations in sedimentation and organic content in five plant associations on a Chesapeake Bay tidal Freshwater Delta. *Estuarine, Coastal and Shelf Science*, *53*, 93–106. https://doi.org/10.1006/ecss.2001.0791

Roelvink, J. A. (2006). Coastal morphodynamic evolution techniques. *Coastal Engineering*, *53*, 277–287. https://doi.org/10.1016/j.coastaleng.2005.10.015

Siobhan Fennessy, M., Brueske, C. C., & Mitsch, W. J. (1994). Sediment deposition patterns in restored freshwater wetlands using sediment traps. *Ecological Engineering*, *3*, 409–428. https://doi.org/10.1016/0925-8574(94)00010-7

Sutherland, J., Peet, A. H., & Soulsby, R. L. (2004). Evaluating the performance of morphological models. *Coastal Engineering*, *51*, 917–939. https://doi.org/10.1016/j.coastaleng.2004.07.015

Temmerman, S., Govers, G., Meire, P., & Wartel, S. (2003a). Modelling long-term tidal marsh growth under changing tidal conditions and suspended sediment concentrations, Scheldt estuary, Belgium. *Marine Geology*, *193*, 151–169. https://doi.org/10.1016/s0025-3227(02)00642-4

Temmerman, S., Govers, G., Wartel, S., & Meire, P. (2003b). Spatial and temporal factors controlling short-term sedimentation in a salt and freshwater tidal marsh, Scheldt estuary, Belgium, SW Netherlands. *Earth Surface Processes and Landforms*, *28*, 739–755. https://doi.org/10.1002/esp.495

Van der Deijl, E. C. (2015). Establishing a sediment budget in the 'Kleine Noordwaard' area of the Biesbosch inland delta. E-proceedings of the 36th IAHR World Congress, 28 june - 3 july, 2015, The Hague, the Netherlands.

Van der Wegen, M., & Jaffe, B. E. (2013). Towards a probabilistic assessment of process-based, morphodynamic models. *Coastal Engineering*, *75*, 52–63. https://doi.org/10.1016/j.coastaleng.2013.01.009

Van der Zon, N. (2013). Kwaliteitsdocument AHN2. *Het Waterschapshuis*, *31*.

Van Rijn, L. (1984). Sediment transport. *Part II: Suspended Load Transport. journal of hydraulic engineering*, *110*, 1613–1641. https://doi.org/10.1061/(ASCE)0733-9429(1984)110:11(1613)

Vandenbruwaene, W., Maris, T., Cox, T. J. S., Cahoon, D. R., Meire, P., & Temmerman, S. (2011). Sedimentation and response to sea-level rise of a restored marsh with reduced tidal exchange: Comparison with a natural tidal marsh. *Geomorphology*, *130*, 115–126. https://doi.org/10.1016/j.geomorph.2011.03.004

Yang, S. L., Zhang, J., Zhu, J., Smith, J. P., Dai, S. B., Gao, A., & Li, P. (2005). Impact of dams on Yangtze River sediment supply to the sea and delta intertidal wetland response. *Journal of Geophysical Research: Earth Surface*, *110*, n/a–n/a. https://doi.org/10.1029/2004JF000271

How to cite this article: Verschelling E, van der Deijl E, van der Perk M, Sloff K, Middelkoop H. Effects of discharge, wind, and tide on sedimentation in a recently restored tidal freshwater wetland. *Hydrological Processes*. 2017;31:2827–2841. https://doi.org/10.1002/hyp.11217

APPENDIX

Sediment balance for all event runs, including the calibration run CA20SMW for reference. Because the calibration run has a different simulation period than the event runs, all terms have been divided by the simulation period T (days) in order to make the numbers comparable. "Mud_in": total inflow of mud divided by T, "Mud_out": total outflow of mud divided by T, %RET: percentage of Mud_in retained in the study area during the simulation. Sand_dS: total net deposition of sand divided by T; dELEV chnls & flats: net total change of the surface level in the channels and the flats divided by T.

Event	Q_lobith (m^3/s)	Wind dir	Wind speed (m/s)	Sea water level	Mud_in (mg/day)	Mud_out (mg/day)	Mud_ret (%)	Sand_dS (mg/day)	dELV_chnls (µm/day)	dELV_flats (µm/day)
CALIBR	N/A	Meas	Meas	N/A	168.7	101.4	40%	−8.4	30.4	16.8
DISCH0	Average (2300)	—	—	astr	236.4	161.8	32%	−0.1	−0.6	30.0
DISCH1	T1 wave (5893 max)	—	—	astr	415.8	302.9	27%	−51.7	−18.4	47.4
DISCH2	T50 wave (11762 max)	—	—	astr	1789.9	1537.1	14%	−433.0	−27.9	114.3
WIND1	Average (2300)	SW	T1 (17.9)	astr + surge	233.3	206.5	11%	−0.4	39.4	-16.2
WIND2	Average (2300)	NW	T1 (14.4)	astr + surge	240.2	197.3	18%	−0.5	20.6	-2.5
WIND3	Average (2300)	NE	T1 (11.8)	astr + surge	236.5	199.0	16%	−0.2	18.5	-4.2
WIND4	Average (2300)	SE	T1 (9.3)	astr + surge	234.1	170.3	27%	−0.2	12.8	10.5
TIDE1	Average (2300)	SW	T1 (17.9)	astr + surge + NT	233.5	206.7	11%	−0.3	37.8	-15.7
TIDE2	Average (2300)	SW	T1 (17.9)	astr + surge + ST	232.9	206.2	11%	−0.2	33.5	-14.5
TIDE3	T1 wave (5893 max)	—	—	astr + NT	416.0	301.8	27%	−45.2	−10.4	46.8
TIDE4	T1 wave (5893 max)	—	—	astr + ST	416.1	303.5	27%	−60.7	−21.0	46.8
COMB1	T1 wave (5893 max)	SW	T1 (17.9)	astr + surge	417.0	378.2	9%	−50.9	−0.5	5.0
COMB2	T1 wave (5893 max)	SW	T(1/25; 6.4)	astr + surge	417.0	307.9	26%	−51.9	−17.7	45.3
WIND5	Average (2300)	SW	T50 (24.3)	astr + surge	228.7	240.3	−5%	40.2	69.8	−39.3